# A Case Study of the Summertime Great Plains Low Level Jet

THOMAS R. PARISH, ALFRED R. RODI AND RICHARD D. CLARK

*University of Wyoming, Department of Atmospheric Science, Laramie, Wyoming*

(Manuscript received 6 February 1987, in final form 12 June 1987)

ABSTRACT

A case study of the kinematical and dynamical evolution of the summertime Great Plains low level jet (LLJ) is presented. Airborne radar altimetry was used to discern the $x$ and $y$ components of the geostrophic wind at three levels in the lower atmosphere throughout the LLJ episode. Results appear to confirm previous theoretical and numerical studies regarding the importance of the diurnal cycle of heating over sloping terrain in producing an oscillating horizontal pressure gradient force. Inertial turning of the LLJ as a result of frictional decoupling was also documented. It is concluded that the inertial oscillations resulting from the sudden decrease in friction in the lower atmosphere during the early evening is the dominant mechanism in forcing this example of a summertime Great Plains LLJ.

## 1. Introduction

One of the prominent meteorological phenomena of the central United States is the so-called Great Plains low level jet (LLJ). Observations have shown that the LLJ is present over a broad horizontal scale from the sloping plains just east of the Rocky Mountains to the Mississippi River. Wind profiles reveal a speed maximum below 1500 m and often no more than 300 m above ground level with a magnitude commonly in excess of 25 m $s^{-1}$. The LLJ undergoes a well-documented diurnal change; often the LLJ has an incoherent structure during the daytime hours, becoming well organized by early evening. The LLJ orientation also displays a significant diurnal change shifting from a southerly direction in the early evening to a southwesterly or westerly direction by morning.

Much of the early documentation of the LLJ occurred as a result of the Great Plains Turbulence Field Program at O'Neill, Nebraska in the early 1950s (Lettau and Davidson, 1957). Swarms of pilot balloons (pibals) were used to discern the temporal and vertical changes in the windfield. A subsequent detailed study of the LLJ using a line of 13 pibal stations stretching from Amarillo, Texas to Little Rock, Arkansas, was conducted in the spring of 1961 (Hoecker, 1963). Results of the study clearly showed the broad horizontal extent of the LLJ over the sloping terrain and the very sharp vertical gradients associated with the jet. Wind speed maxima were observed between 300–800 m above ground level and speeds as much as 1.95 times the geostrophic values were reported. A comprehensive LLJ climatology is presented in Bonner (1968). The study incorporates a two-year record (1959–60) of wind data from 47 rawinsonde stations in the United States in order to depict geographical and diurnal variations of the LLJ and to determine the maximum frequency of occurrence. The results suggest the LLJ frequency maxima is centered over the Oklahoma–Kansas region of the Great Plains; a LLJ was identified on about 80% of the 0600 CST summertime (April–September) soundings at stations along the Great Plains for the two-year period.

Numerous theories have been proposed to explain the development and evolution of the Great Plains LLJ. Blackadar (1957) considered the nocturnal supergeostrophic wind maximum to be the result of an inertial oscillation, induced by the sudden cessation of turbulent mixing in the lower boundary layer after sunset. He notes that the jet is frequently observed at the top of the nocturnal inversion and that the ageostrophic components are largest in the lower levels and decrease sharply with height. A different boundary layer explanation was offered by Wexler (1961). He notes the LLJ is analogous to western boundary currents in the ocean such as the Gulf Stream. According to Wexler, the Rocky Mountain complex acts as a barrier to the westward flowing tradewinds, deflecting air northward in advance of the mountainous terrain. Using the potential vorticity equation, he argues the northward trajectory of the air currents implies intensification and development of a jet feature.

Holton (1967) examined the role of the terrain slope in producing the LLJ. Using a coupled thermal–viscous boundary layer system of equations, he shows that the thermal effects can contribute substantially to the amplitude of the diurnal wind oscillation over sloping terrain. A similar line of reasoning can be found in Hoecker (1965). An analysis by Bonner and Paegle (1970) suggests that significant diurnal variations of

*Corresponding author address:* Dr. Thomas R. Parish, Dept. of Atmospheric Science, University of Wyoming, Box 3038, Laramie, WY 82071.

the geostrophic wind occur over the south central United States. They attribute such variations to the periodic changes in the thermal wind resulting from the diurnal cycle of heating and cooling of the sloping terrain. Their results indicate a surface geostrophic wind oscillation with an amplitude reaching 5 m $s^{-1}$ with the maximum southerly geostrophic wind occurring in the later afternoon and the minimum during the early morning hours. A numerical study of the LLJ is presented in McNider and Pielke (1981). The results seem to confirm previous studies regarding the oscillation in the horizontal pressure gradient due to the temperature evolution over the sloping terrain. The terrain-induced thermal wind changes direction from the north during daytime hours to the south at night. Model results suggest the surface geostrophic wind oscillation may be up to 6 m $s^{-1}$. McNider and Pielke conclude that the development of the terrain-induced pressure gradient force is a significant forcing mechanism in the evolution of the LLJ.

While boundary layer processes have been emphasized in literature pertaining to the LLJ, Uccellini and Johnson (1979) point out that in some cases upper and lower tropospheric jets are intimately coupled as a result of the indirect circulation and corresponding mass adjustments in the exit region of the upper level jet streak. Uccellini (1980) has reviewed a number of LLJ cases previously discussed in the literature and concludes that in 12 out of 15 cases a propagating upper level jet streak was present. He notes that subsynoptic mass adjustment processes associated with leeside cyclogenesis can be an important factor in LLJ development. Under such conditions the LLJ does not display the marked diurnal oscillation and can be situated as high as the 850 mb level.

This dichotomy in the forcing mechanisms has led to some confusion over the term "low level jet." In the case study to follow, data were collected during 23–24 July 1983. The synoptic forcing was very weak throughout the period with an upper level high pressure ridge present over the central United States. The LLJ is therefore a classic example of boundary layer forced dynamics rather than the type discussed in Uccellini and Johnson (1979).

The purpose of this paper is to report on direct measurements of the horizontal pressure gradient evolution and consequently the ageostrophic wind in the lower atmosphere during a LLJ episode.

## 2. Discussion of data collection

During July 1983, a field project was conducted in north central Oklahoma to monitor the kinematic and dynamic evolution of the Great Plains LLJ. The primary database was obtained using the University of Wyoming Beechcraft Super King Air (K/A) instrumented research aircraft. Stimulus for the experiment came from the realization that precise and high resolution radar altimeters and navigational aids such as the inertial navigation system (INS) on research aircraft had the potential for measuring the slope of isobaric heights on the 100-km scale. Brown et al. (1981) have described the application of modern aircraft instrumentation to geostrophic wind measurements. As shown in Fig. 1, the research aircraft flies at constant pressure and the height above the terrain is measured by the radar altimeter. Minor excursions of the autopilot from the isobaric surface are corrected using the hydrostatic equation. By adding the height of the underlying terrain obtained from navigational positioning estimates to the radar altitudes, the height of the isobaric surface is obtained. This technique has been used by Shapiro and Kennedy (1981, 1982) to study midlatitude jet stream dynamics over the ocean and over complex terrain. They estimate errors in isobaric heights to be ±6 m over the ocean and ±10 m over land. These error margins are acceptable for upper tropospheric jet stream studies since isobaric slopes approach $10^{-3}$ (see Fig. 5 in Shapiro and Kennedy, 1982). However, for mesoscale events having characteristic length scales less than 100 km and wind speeds on the order of 10 m $s^{-1}$ or less, such errors are of the same magnitude as the isobaric slope signal itself and more precision is required. A technological description of the geostrophic wind calculations, limitations and system errors are discussed in Rodi and Parish (1987). In general, errors in the geostrophic wind calculations are shown to be on the order of ±1 m $s^{-1}$ over the 100 km scale, implying the aircraft is able to track the isobaric surface over 100 km scales with a fidelity of less than 1 m.

A total of four complete episodes of the LLJ evolution were documented during the month-long field experiment. Each case study period covered the entire nighttime LLJ evolution, beginning generally around 1600

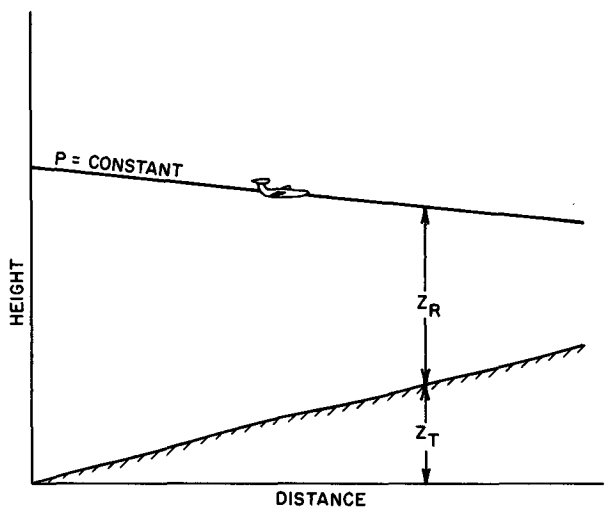


FIG. 1. Schematic of airborne radar altimetry. The height of the isobaric surface is obtained by adding the radar altitude ($Z_r$) with the terrain height above sea level ($Z_t$).

LT and ending about 0800 LT the next morning. Three flights, each of 5 h duration, were conducted during this period. Therefore, the aircraft was collecting data nearly continuously during the LLJ episode. To study the vertical structure of the LLJ a number of soundings to approximately 750 mb were conducted. In addition, three different levels were flown in an alternating fashion throughout the night. The flight strategy consisted of an L-shaped series of predetermined legs of approximately 100 km in length at three levels in the lower atmosphere. The particular flight level selection was based on knowledge of and/or forecast position of the LLJ core. During the 23 July case study, flight legs were conducted approximately 300, 600 and 900 m above ground level. To facilitate navigational positioning, flight legs followed well-defined north–south and east–west trending highways. Event markers input from the flight scientists were recorded on tape to indicate the start and end of each leg. Visual checks were possible throughout the observing period owing to headlights from oncoming cars and illumination from the near-full moon. The project location and flight strategy are illustrated in Fig. 2.

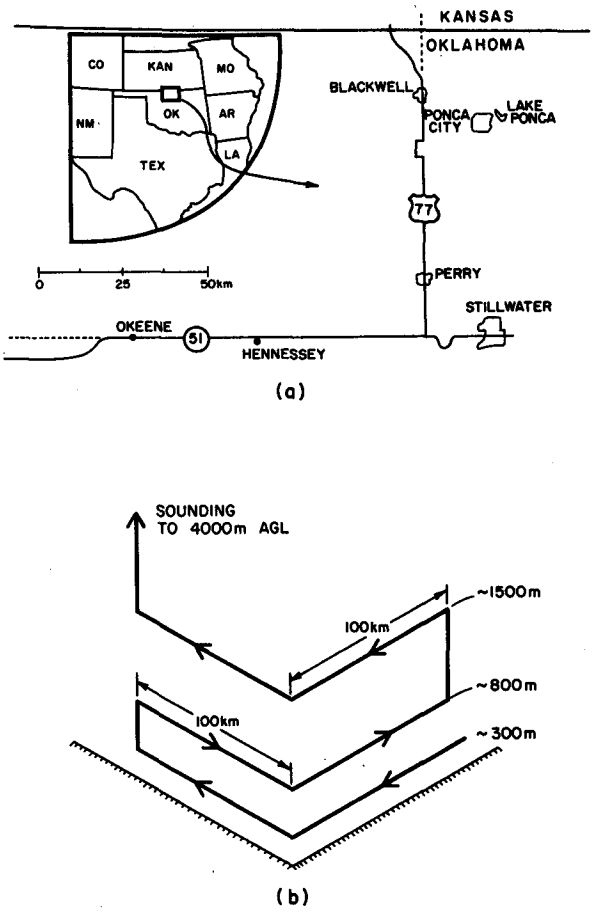


FIG. 2. The LLJ field project location (top) and flight strategy (bottom).

## 3. The 23 July 1983 case study

### *a. Kinematic LLJ structure and evolution*

The large-scale synoptic conditions for the 23 July 1983 case study are revealed in the 300 mb map (Fig. 3a). A broad region of high pressure is present over much of the southern United States and near-barotropic conditions exist throughout the upper troposphere. The 700 mb map for the same time (Fig. 3b) also shows relatively little large-scale forcing. As well, an analysis of surface barograms and hourly temperature data for NWS stations within a 300 km radius of the study area indicated no appreciable synoptic drift during the case study (Clark, 1987). Weak southerly flow is present over much of the southern Great Plains in association with the high pressure cell over the Gulf of Mexico. Owing to the nearly absent large-scale forcing mechanisms, development of the LLJ is due to boundary layer processes and consequently large diurnal changes are to be expected.

The kinematic evolution of the LLJ profile was detected by a series of K/A soundings throughout the night. The climb rate was limited to approximately 150 m $min^{-1}$ in order to maintain the fidelity of the INS-derived wind measurements. A sample of the soundings of the $u$ and $v$ scalar motion components and potential temperature is shown in Fig. 4. At the time of the climbout sounding (Fig. 4a), the boundary layer was characterized by a deep adiabatic layer extending past 750 mb. The characteristic LLJ signature was not present during this late afternoon sounding and both the $u$ and $v$ components displayed a rather incoherent vertical structure. By 2030 LT, the LLJ begins to develop (Fig. 4b). The narrow jetlike structure is clearly seen in the $v$ component. In addition, the $u$ component in the lower levels of the atmosphere shows evidence of inertial turning; the magnitude of the $u$ component wind profile below about 870 mb has decreased from the earlier sounding. Also, the potential temperature profile indicates the atmosphere has become more stable due to the radiational cooling in the lower levels during the evening.

By 0230 LT 24 July 1983, a classic boundary layer jet is revealed (Fig. 4c). The $v$ component of motion profile shows a well-developed jet located about 300 m above ground level with a magnitude in excess of 15 m $s^{-1}$. The $u$ component profile is suggestive of further pseudo-inertial turning compared to the profile in Fig. 4b some 6 hours earlier. Note that the LLJ at this time nearly fits the Bonner (1968) criterion 3, the most developed LLJ hierarchial classification. The potential temperature profile shows continual stabilization, especially below the 880 mb level.

Figure 4d illustrates the profiles of the $u$ and $v$ motion components and potential temperature at 0730 LT. Although the sun has been up for nearly two hours and the wind profiles are starting to decay, most of the LLJ features are still prominent. The wind profiles in-

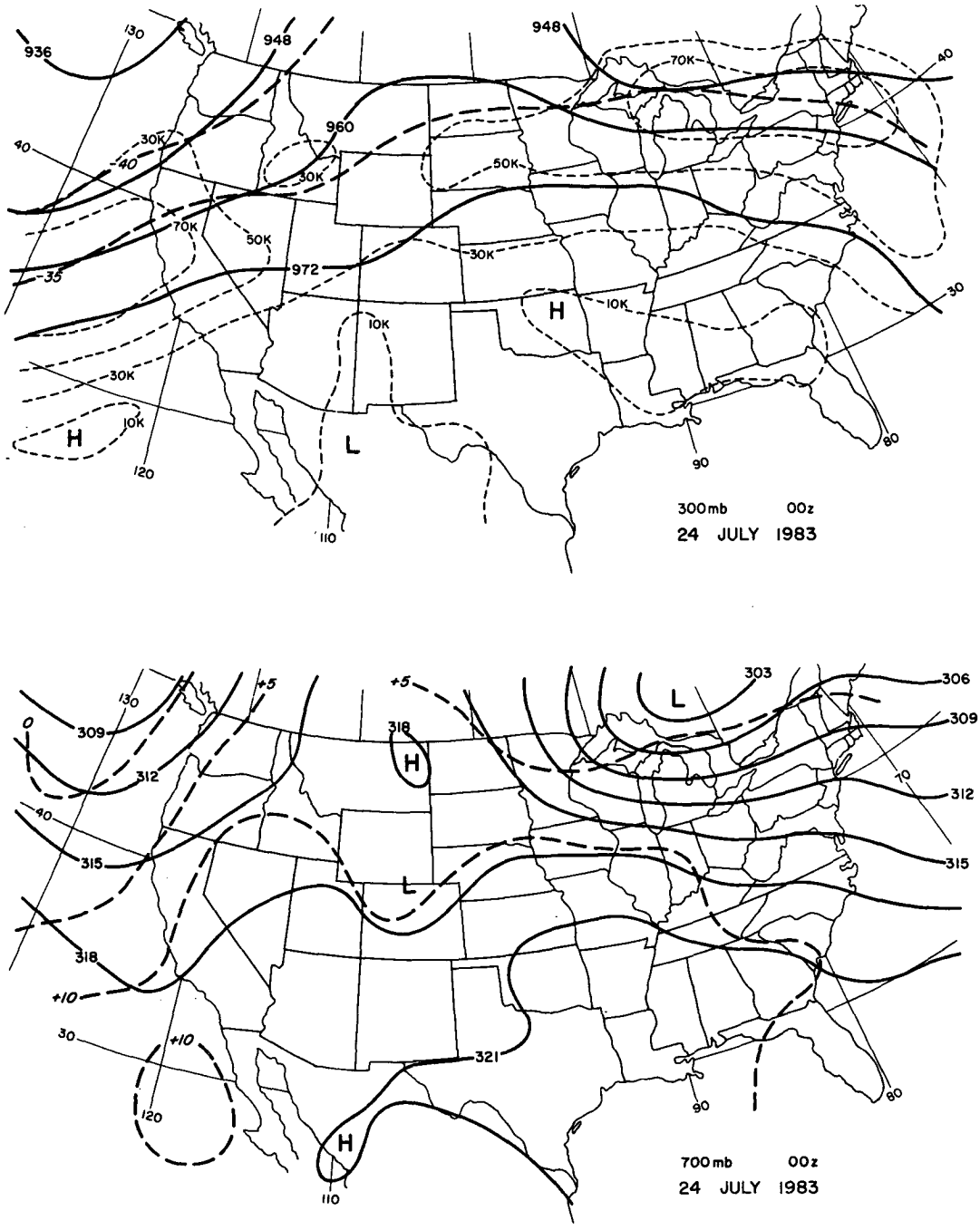


FIG. 3. (a) 300 mb map for 00Z 24 July and (b) 700 mb map for 00Z 24 July.

dicate a continued clockwise turning of the ageostrophic component with time and the LLJ is now directed in a near west-to-east fashion. Even at this time the LLJ is extremely sharp and well developed with a magnitude of about 17 m $s^{-1}$ at the core dropping to about 5 m $s^{-1}$ at the 800 mb level. The thermal stratification in the potential temperature profile reveals a layer of relatively intense nocturnal radiational cooling extending from the surface to approximately 800 m near the 890 mb level.

The picture set forth for this 23 July 1983 case study is one of classic LLJ development. The hodographs for all three flight levels shown in Fig. 5 are similar to those shown by Izumi and Barad (1963) and the ageostrophic hodographs presented in Blackadar (1957). A systematic decrease in the ageostrophic nature of the

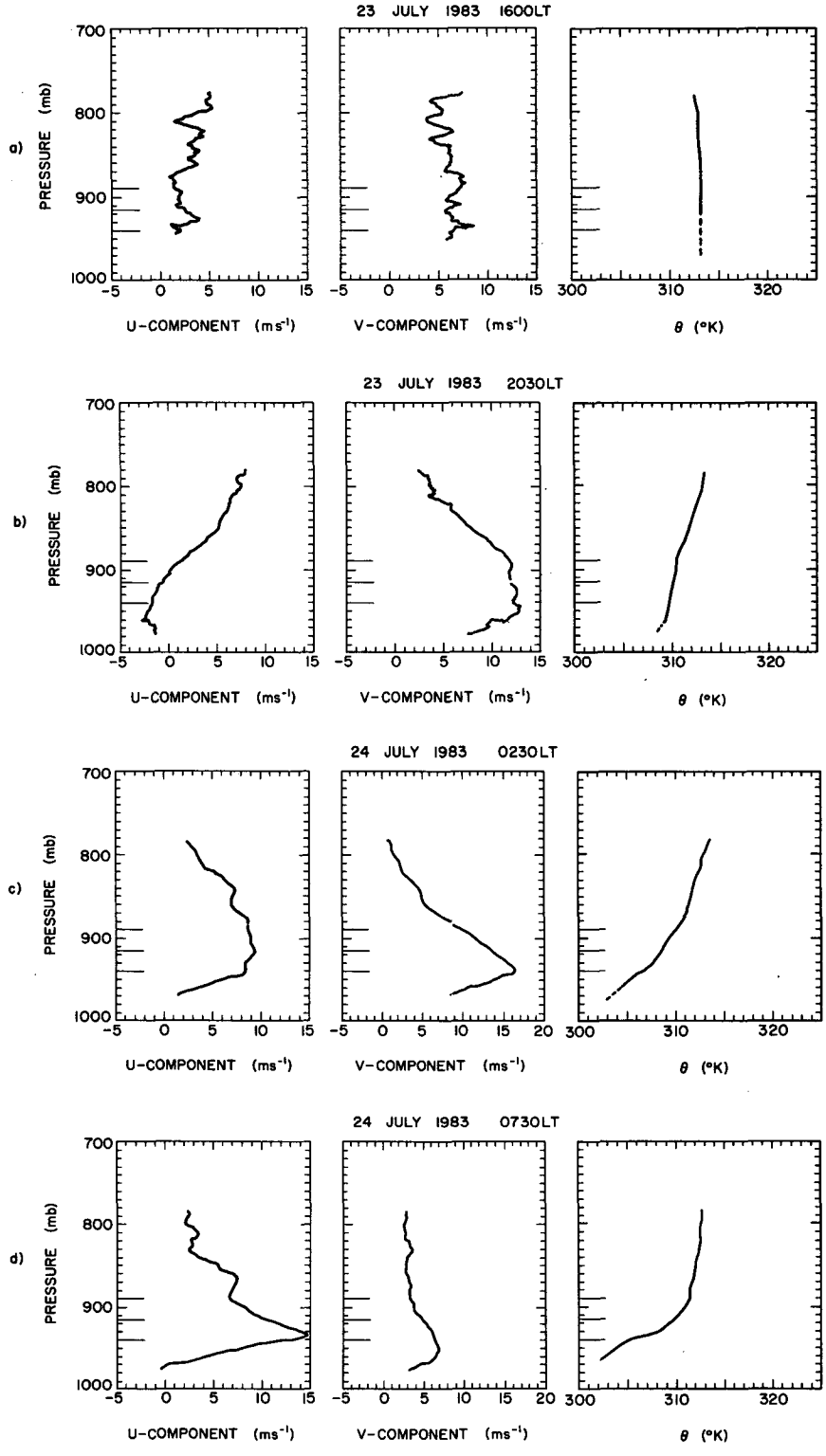


FIG. 4. Soundings to approximately 750 mb for the $u$ and $v$ wind components and potential temperature at (a) 1600 LT, (b) 2030 LT, (c) 0230 LT and (d) 0730 LT for the 23–24 July case study. Horizontal bars on ordinate indicate flight levels.

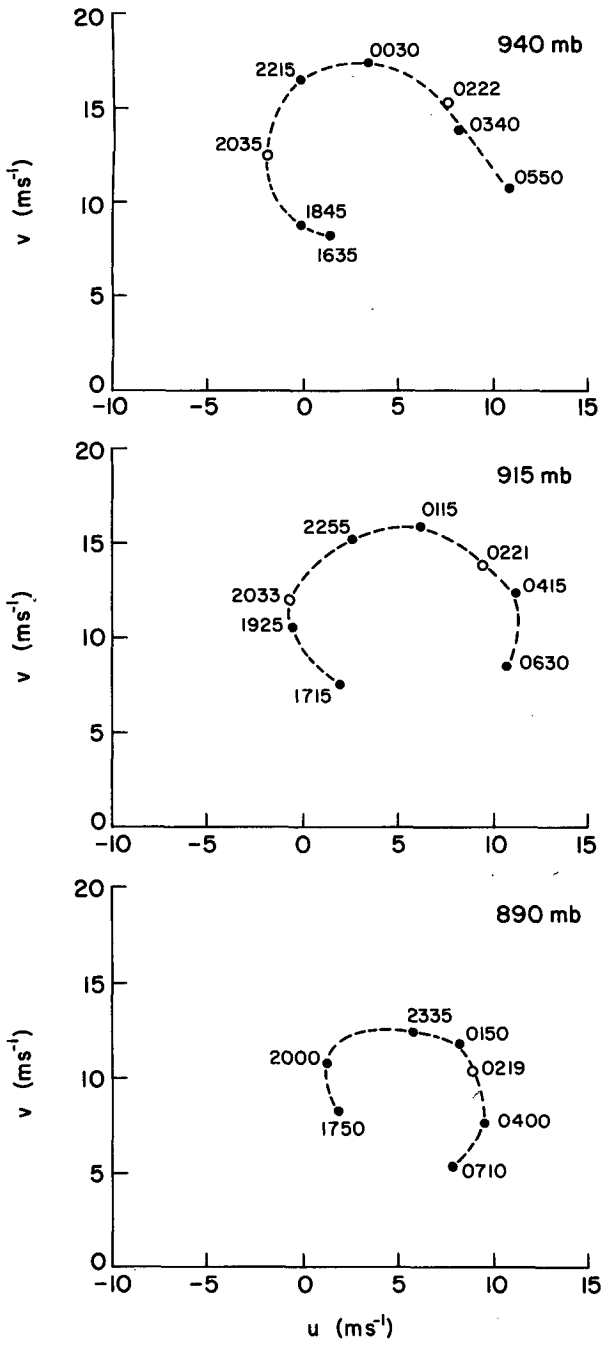


FIG. 5. Hodographs of the time evolution of the LLJ at 940, 915 and 890 mb levels.

wind with height is present. The veering of the winds at each level with time is highly suggestive of the inertial turning mechanism proposed by Blackadar (1957).

### b. *Forcing of the LLJ*

Two important forcing mechanisms have been proposed in literature pertaining to the summertime Great Plains LLJ: frictional decoupling and evolving horizontal pressure gradients. The rapid decay of the convective boundary layer in the early evening after sunset and consequently the sudden decrease in the friction force produces an inertial oscillation as the wind attempts to adjust to the pressure gradient force. Also, the diurnal pattern of heating and cooling of the sloping terrain produces a terrain-induced pressure gradient force which undergoes a periodic behavior. For the most part, terrain slopes over the Great Plains are oriented east–west and influence the pressure gradient force in the $x$-direction or the $v$ component of the geostrophic wind. During the daytime, solar insolation of the sloping terrain results in sloped-inversion pressure gradient force directed westward tending to produce an enhanced southerly geostrophic component. At night, radiational flux divergence at the surface results in cooling of air adjacent to the terrain slopes and thus creating a horizontal pressure gradient force directed to the east. The maximum amplitudes of such terrain-induced geostrophic winds occur in late afternoon and just before dawn.

Measurement of these forcing parameters is understandably difficult owing to the extremely small magnitudes involved and inherently large uncertainties in conventional instrumentation. No direct measurement of friction was attempted in the study although a proxy indicator is available in the MRI turbulence probe which measures turbulent intensity. In a qualitative sense, the evolution of turbulent intensity is an indication of frictional changes. This measure provides a qualitative check of the frictional decoupling mechanism in the lower atmosphere which occurs in the early evening. An ensemble of vertical profiles of the eddy dissipation rate measured during the K/A soundings throughout the LLJ episode for the 23 July case study is illustrated in Fig. 6. Relatively large values of the eddy dissipation rate are found in the lower atmosphere during the late afternoon (Fig. 6a) with values between $10^{-3}$ and $10^{-2}$ m$^2$ s$^{-3}$. The turbulent intensity level drops off sharply in the early evening; by 2030 LT the eddy dissipation rates in the layer from about 970 to 870 mb have been reduced by nearly two orders of magnitude, varying between approximately $10^{-5}$ and $5 \times 10^{-5}$ m$^2$ s$^{-3}$. Six hours later at 0230 LT (Fig. 6c) the vertical profile of eddy dissipation rate has decreased an additional two orders of magnitude between approximately 925 and 850 mb. Values of $\epsilon$ show an increase during this time period in the 940–960 mb layer in response to the mechanically induced turbulence associated with the strong vertical wind shear of the well-developed LLJ. By 0730 (Fig. 6d), the turbulence levels are clearly increasing owing to the incident solar radiation and strong heating at the surface. The evolution of the eddy dissipation rate and corresponding changes in the wind profiles throughout the early evening as illustrated in Fig. 4 offer strong support for the importance of the frictional decoupling mechanism

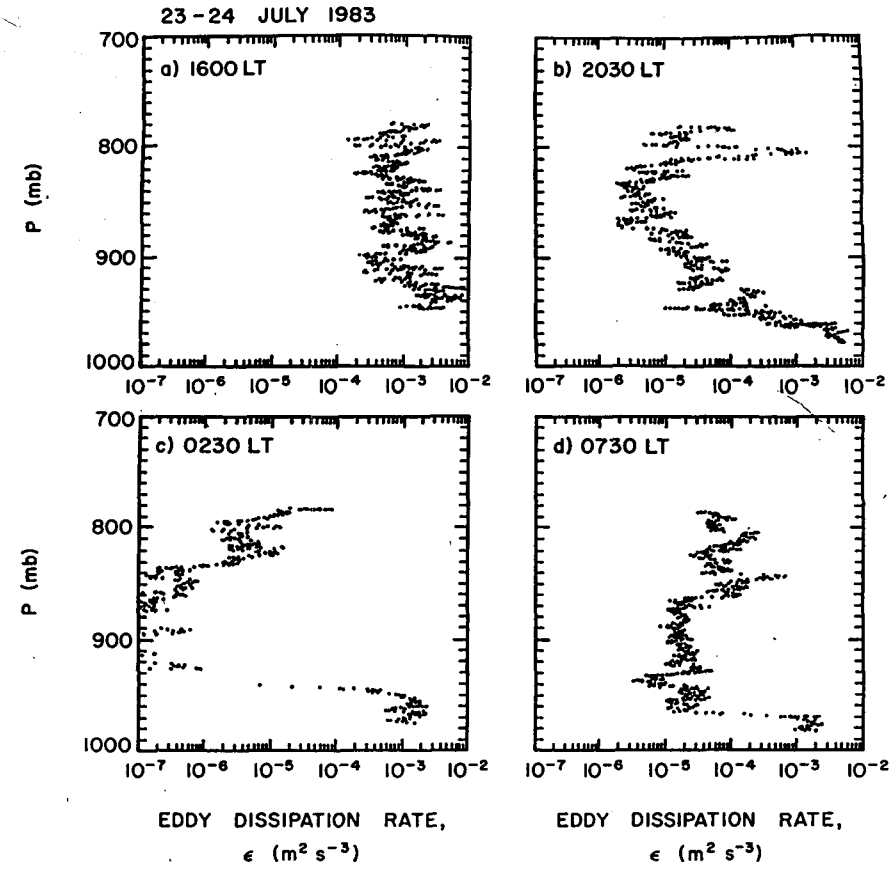


FIG. 6. Vertical profiles of eddy dissipation rate for the 23–24 July 1983 case study.

proposed by Blackadar (1957) in shaping the development of the LLJ. As can be verified by comparing Figs. 4 and 6, a strong relationship exists between the wind evolution and the changes in turbulent intensity levels.

As discussed in the previous section, strong emphasis was placed on direct measurements of isobaric slopes and, consequently, the geostrophic wind. The flight legs shown in Fig. 2 were designed to provide optimal coverage of evolutionary changes in both the $x$ and $y$ scalar components of the pressure gradient force. It should again be pointed out that the large-scale horizontal pressure gradient force in the free atmosphere was quite weak, supporting only a southwest geostrophic wind of 5–10 m $s^{-1}$. A total of six independent measures of the component geostrophic wind were made for each of the three levels over the duration of the LLJ episode. As is to be expected, the $x$ component of the horizontal pressure gradient is generally larger than the $y$ component. However, both 100-km legs are flown over very complex terrain. Solar insolation and nocturnal radiational cooling of the smaller scale terrain slope features appear to produce observable oscillatory features in the isobaric height trace. The 100 km scale horizontal pressure gradients present must be viewed with this in mind. The geostrophic winds measured are averages over the entire leg and mask the often complicated isobaric slope structure. Significant fluctuations of the horizontal pressure gradient force on time and space scales less than 15 min and 100 km are common. As discussed in Rodi and Parish (1988), the instrumented aircraft measurement platform is able to track the isobaric surface with a very high degree of precision. However, interpretation of these results is still sensitive to boundary layer processes and large-scale forcing. For example, pressure changes at the surface amounting to only tenths of millibars per hour can introduce complications in the isobaric slope detection since the isobaric surface is changing in altitude with time in response to the pressure change. The 100 km legs require flight times on the order of 18–20 min. During such time intervals, the movement of the isobaric surface heights introduces an error in the geostrophic wind calculations and illustrates a weakness of time–space transformations. Such high resolution pressure change effects must be incorporated to achieve representative estimates of geostrophic winds. For the 23 July 1983 case study, the evolution of the mean height above

ground level for each leg was determined and corrections have been applied to correct for vertical displacement of the pressure surfaces. A detailed summary of sources of error in the isobaric slope detection technique is given in Rodi and Parish (1988).

An example of the geostrophic wind measurement for the 940 mb east–west leg is shown in the series of traces in Fig. 7. The top trace (Fig. 7a) shows the radar altitudes of the underlying terrain. East is to the left for all east–west traces. As can be seen from Fig. 7a, the terrain heights gradually increase from east to west with considerable small-scale variability. The radar altitudes are near-mirror images of the underlying terrain structure (Fig. 7b). The terrain heights are obtained in a two-step fashion. As discussed in Rodi and Parish (1988), refined navigational positioning is necessary for proper isobaric height determination. To improve on the INS position estimates, the distance measuring equipment (DME) signal is used to damp oscillations in the INS. The terrain heights are then obtained using the refined position estimates and interpolation from the USGS 7.5 min topographic maps. All processing is done by computer. As a means to check on the positioning, small random errors in both latitude and longitude are assumed and a series of comparisons are made between the radar altitude and underlying terrain features. The assumed correct position shows the characteristic mirror images between the terrain and radar altimeter signal as illustrated in Fig. 7.

The height of the isobaric surface (Fig. 7c) is then simply the sum of the radar altitude and height above sea level of the underlying terrain. The straight line represents a least-squares linear fit to the data, the slope representing the isobaric slope and, thus, the geostrophic wind. In this case, the geostrophic wind is 15.1 m $s^{-1}$ with an error of $\pm 0.6$ m $s^{-1}$ which is significant to the 95% confidence level assuming a normal distribution of the errors. This horizontal pressure gradient measurement approximately represents the largest magnitude of the geostrophic wind since the flight times of 1636–1653 LT are near the time of maximum temperatures.

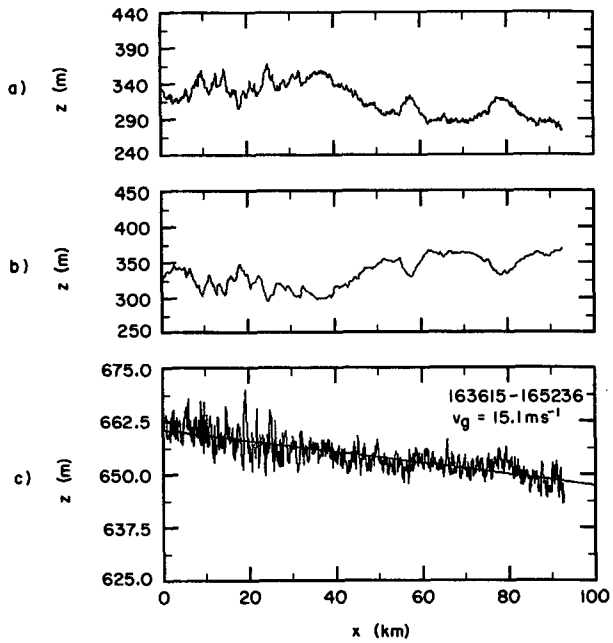


FIG. 7. (a) Radar altitude overlying (b) terrain height, and (c) isobaric height trace obtained from research aircraft observation platform for the 940 mb east–west leg 1636:15–1652:36 23 July 1983.

The second east–west leg at the 940 mb level occurred approximately two hours later (1824–1842 LT). The traces of radar altitude, underlying terrain height and resulting isobaric surface heights are shown in Fig. 8. Again, a very coherent signal is obtainable. The magnitude of the geostrophic wind has decreased slightly to a value of 14.6 m $s^{-1}$ with an error of $\pm 0.7$ m $s^{-1}$ again assuming a 95% confidence level and that errors are normally distributed. Isobaric height traces for the four remaining east–west legs at the 940 mb level are illustrated in Fig. 9. Traces of radar altitudes and underlying terrain heights are nearly identical to those shown in Figs. 7 and 8 and are not included. A systematic decrease in the $v$ component of the geostrophic wind can be seen from this series. The oscillation of the geostrophic wind amplitude amounts to approximately 3 m $s^{-1}$ which is similar to the magnitude of the surface geostrophic wind oscillation reported by McNider and Pielke (1981). Errors in the isobaric slopes in all cases are less than 0.75 m $s^{-1}$ again assuming a 95% confidence level and normally distributed errors.

Analyses such as those shown in Figs. 7–9 have been completed for both $x$ and $y$ components at the 940, 915 and 890 mb levels for a total of 36 100 km average geostrophic wind measurements. The largest errors encountered in the isobaric slope calculations correspond to less than a 0.90 m $s^{-1}$ error in the geostrophic wind again assuming a 95% confidence level. The evolution of the geostrophic wind components at the different levels are illustrated in Fig. 10. Clearly evident is the decreasing trend in the $y$ component geostrophic wind values throughout the evening and early morning hours at all levels. The largest pressure gradients are seen at the lowest level (940 mb) although the actual oscillations in the $y$ component of the geostrophic wind magnitude at 940 and 915 mb are comparable. The 890 mb series of $v_g$ measurements is puzzling. The isobaric height analysis for each leg shows the airborne instrumentation platform is able to track the isobaric surface with extreme fidelity. The oscillatory pattern observed in the geostrophic component magnitudes may be the result of pressure changes owing from the mutual adjustment of the mass and wind field on a time scale not resolvable by this study. Because the flight legs were separated by at least two hour intervals, it was necessary to interpolate linearly between flight legs to estimate

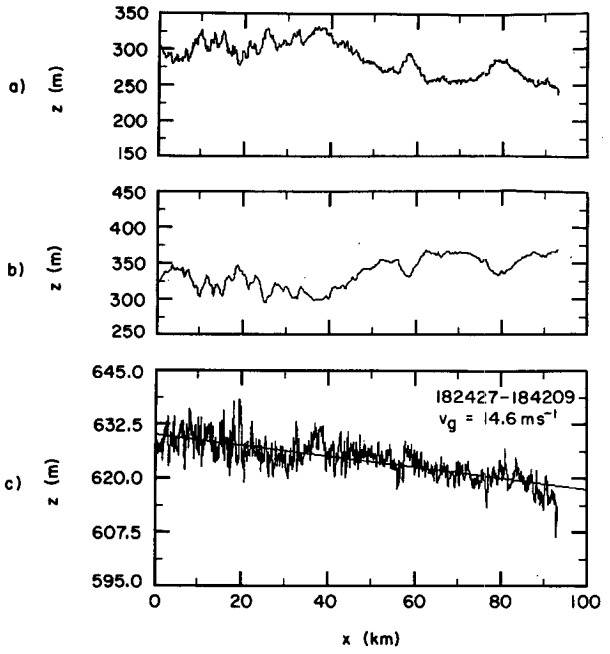


FIG. 8. As in Fig. 7 except for 1824:27–1842:09 23 July 1983.

the in-flight changes in the isobaric heights. Hourly surface pressure and altimeter readings were also available, yet the imprecise knowledge of the evolving thermal structure between the surface and the 890 mb flight level precluded further refinement of the small isobaric height changes. Another possible explanation for the complex behavior of the east–west pressure gradients could be transient inertia–gravity wave phenomena. The 890 mb level approximately represents the top of the nocturnal boundary layer (Fig. 4c). Introduction of such wavelike features could significantly disrupt measurements of isobaric slopes. At present, it is impossible to determine a causal mechanism uniquely. However, the unusual behavior of the east–west pressure gradients does not seem to be the result of the instrumentation platform.

Aside from the well-established decrease of the $y$ component of the geostrophic wind, the most prominent feature illustrated in Fig. 10 is the decrease of the $x$ component of the geostrophic wind. This decrease is documented at each of the three levels and is thought to be the result of synoptic scale influences. This suggests that the time evolution of both components of the geostrophic wind may include large scale effects. There appears to be a slight drift in the pressure gradients in the free atmosphere during the case study observing period. It is difficult to sort the terrain-induced geostrophic wind tendencies from synoptic changes. However, upper level maps suggest the large-scale pressure gradient changes are small. The 850 mb maps for this period show only a slight relaxation of the already weak gradients over the Oklahoma region. In addition, the north–south terrain profile is quite irregular and boundary layer processes may play a role. The steepest 25 km stretch is located near the south end of the north–south leg. The irregular patterns of heating and cooling of the terrain may introduce complex small-scale features which are of a magnitude easily discernable from the instrumentation platform.

It is believed that the geostrophic wind tendencies in Fig. 10 can be attributed primarily to the dynamics of heating and cooling over the sloping terrain. Another relevant measure of this terrain-induced forcing is the thermal wind. Since the flight legs are along isobaric surfaces, the variation of temperature observed over the 100-km pass is a direct measure of the thermal wind. Some synoptic influences again may be present, yet the evidence strongly suggests the underlying terrain is primarily responsible for the observed temperature

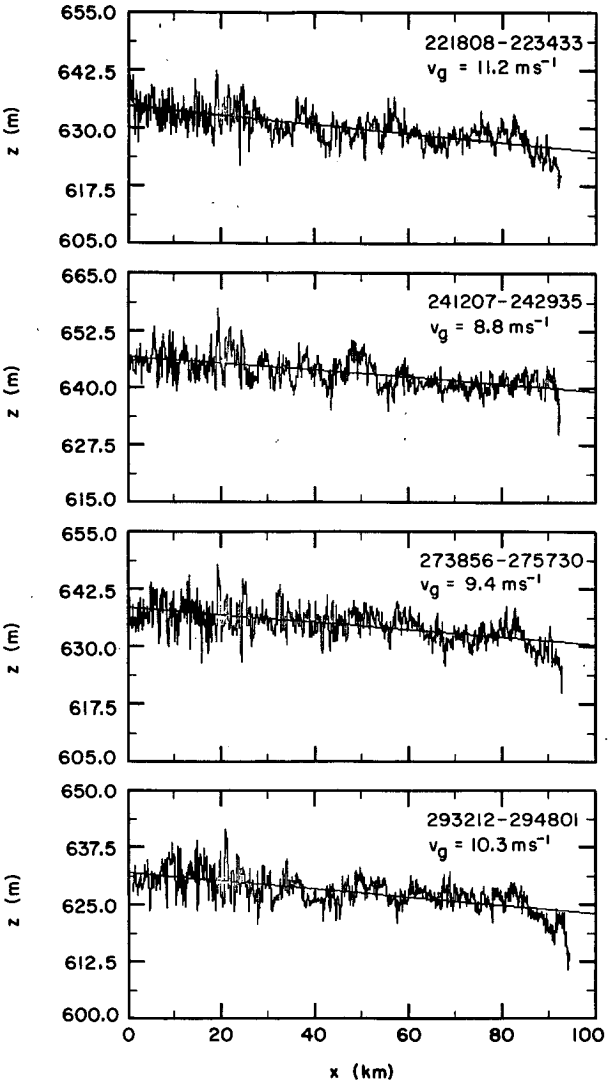


FIG. 9. Isobaric height traces for the 940 mb east–west legs.

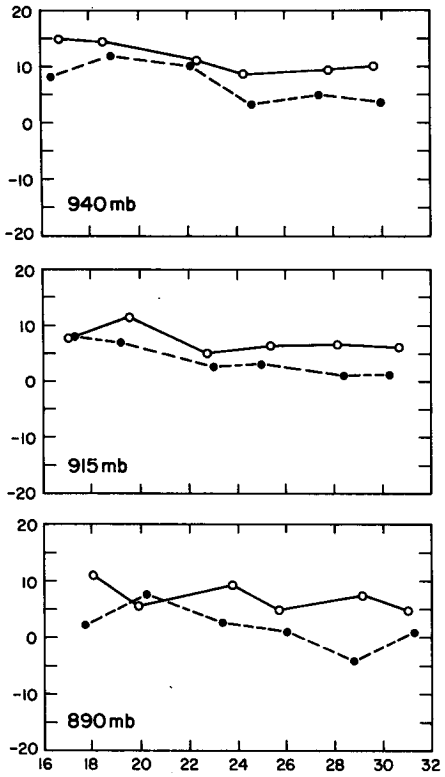


FIG. 10. Time evolution of $x$ (dashed line) and $y$ (solid line) geostrophic wind components derived from airborne radar altimetry for 940, 915 and 890 mb levels.

variations. To illustrate, Fig. 11 shows the temperature changes along the east–west legs for the 940 and 890 mb levels throughout the entire LLJ episode. During the late afternoon and early evening hours, a distinct east-to-west temperature increase of approximately 3°C/100 km is observed at both the 940 and 890 mb levels. This northerly thermal wind is to be expected; the strongest heating occurs at the surface which slopes upward to the west, implying the temperatures should increase to the west along a constant pressure surface. There is only a suggestion that the 940 mb thermal wind is larger than the 890 mb thermal wind. The strong mixing and resulting adiabatic nature of the lower atmosphere below about 750 mb does not support strong vertical differences in the thermal wind which are well documented in the stable boundary layer (Lettau and Schwerdtfeger, 1967). As evening progresses and the near-surface layer begins to stabilize, the 940 level responds abruptly. In the 4-hr interval from 1830–2230 LT, the isobaric temperature variation is reduced from 3.7°C/100 km to approximately 0.5°C/100 km. As expected, the 890 mb thermal wind becomes reduced but the total change is substantially less than at 940 mb. Such variations in the thermal wind match theoretical expectations and are strongly suggestive of terrain-induced forcing (Clark, 1987). The continued stabilization results in a 940 mb level thermal wind direction reversal, although the magnitude of this southerly thermal wind is only a fraction of the northerly thermal wind observed in the late afternoon. Note that local terrain features result in small-scale drainage flows which lead to temperature perturbations over sections of the 100-km leg. The 890 mb thermal wind does not change sign over the course of the night. This is not totally unexpected. From the soundings shown in Fig. 4, most of the diabatic cooling is restricted below about 900 mb. From 1600 to 0730 LT the following morning, the potential temperature decreases by approximately 8°C at 940 mb but only by 2°–3°C at 890 mb.

Direct measurement of the horizontal pressure gradient force and INS-derived wind measurements allow for determination of the ageostrophic motion components. Because of errors involved with both the isobaric slope detection and INS wind measurements, accuracy of the ageostrophic wind calculations are probably on the order of $\pm 2$ m s$^{-1}$. Despite this error margin, certain features are obvious. Results for the 940 and 915 mb levels are shown in Fig. 12. As is to be expected, ageostrophic components are negative in the early evening and increase during the night in a periodic fashion. The $y$ ageostrophic component reaches a maximum value earlier than the corresponding $x$ ageostrophic component. There appears to be a suggestion that the two ageostrophic components are out of phase by a period of approximately 4–5 h. Theoretical studies indicate the two components should be out of phase by approximately one-quarter of the inertial period which corresponds to 5.1 h. Thus, it appears the ageostrophic profiles illustrated in Fig. 12 are representative of expected values.

From measurements of the horizontal pressure gradients and inferences on the ageostrophic nature of the flow, it is possible to offer a preliminary judgment on the relative importance of the frictional decoupling versus the diabatic process over sloping terrain in forcing the LLJ. In general, the ageostrophic wind is composed of two primary components: the isallobaric component associated with the changing geostrophic wind and the inertial component (Haltner and Martin, 1957). Estimates of the isallobaric components can be obtained from the geostrophic wind measurements in Fig. 10. The results suggest the isallobaric components induced by the relaxing east–west pressure gradients (decreasing southerly geostrophic wind) are largest in the early evening (1830–2400) hours with a magnitude of approximately 3–4 m s$^{-1}$, decreasing to approximately 1–2 m s$^{-1}$ in the early morning hours. It appears the isallobaric components arising from the relaxing of the terrain-induced horizontal pressure gradients are secondary to the frictional-decoupling inertial components in the total ageostrophic wind. Calculations suggest the isallobaric components comprise roughly one-quarter of the ageostrophic wind in the early evening and only 10 percent throughout the early morning

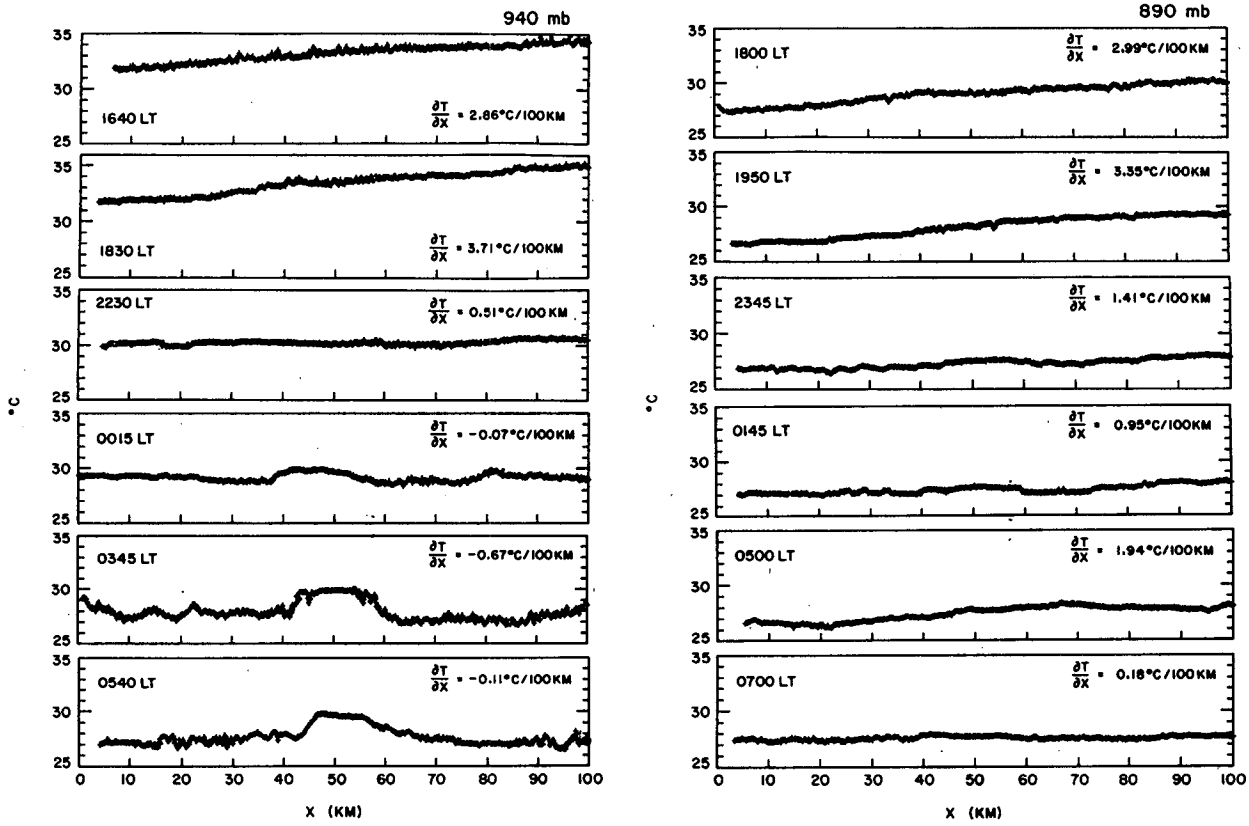


FIG. 11. Time evolution of isobaric temperature gradient for 940 and 890 mb east–west flight legs.

hours. This implies that the frictional decoupling mechanism first proposed by Blackadar (1957) is probably the dominant forcing mechanism for this summertime LLJ case study.

## 4. Implications and conclusions

A detailed case study of one complete episode of the summertime Great Plains LLJ has been presented. Aside from documenting the kinematic structure of the LLJ, emphasis is placed on the dynamics of the heating and cooling of the sloping terrain in an attempt to provide observational support for previous theoretical and numerical studies. The University of Wyoming Beechcraft Super King Air instrumented aircraft observational platform was the main source of data collection.

Airborne radar altimetry has been used in an attempt to discern the forcing mechanisms responsible for the evolution of LLJ. The height of the isobaric surface above sea level is obtained by adding the radar altitude height and the height of the terrain derived from refined navigational positioning of the INS. The slope of the isobaric surface is a measure of the geostrophic wind; a total of six flight passes were conducted over the preselected east–west and north–south legs at 940, 915 and 890 mb to enable the evolution of the geostrophic wind to be monitored.

The resulting kinematic evolution of the LLJ for 23 July 1983 is a classic example of boundary layer forcing. The LLJ becomes coherent early in the evening with the jet core positioned about 300 m above ground level. Also, a well-defined pseudo-inertial turning of the wind is evident. The LLJ winds shift from a southerly direction early in the evening to nearly a westerly direction by dawn. Results from the horizontal pressure gradient force measurements clearly suggest a relaxation in the geostrophic wind over the east–west leg during the evening hours similar to that reported by McNider and Pielke (1981) although synoptic influences may be present as well. The largest pressure gradients are clearly seen to be at the lowest level, again in agreement with previous studies. However, the measurements also underscore the complexity and possible short time scale transient behavior of the adjustment process occurring after sunset in the lower levels of the atmosphere over the Great Plains. Small pressure changes at the surface corresponding to local height changes in the isobaric surfaces were evident throughout the night. Corrections need to be applied to account for the in-flight changes in the height of the isobaric surface in order to arrive at a representative

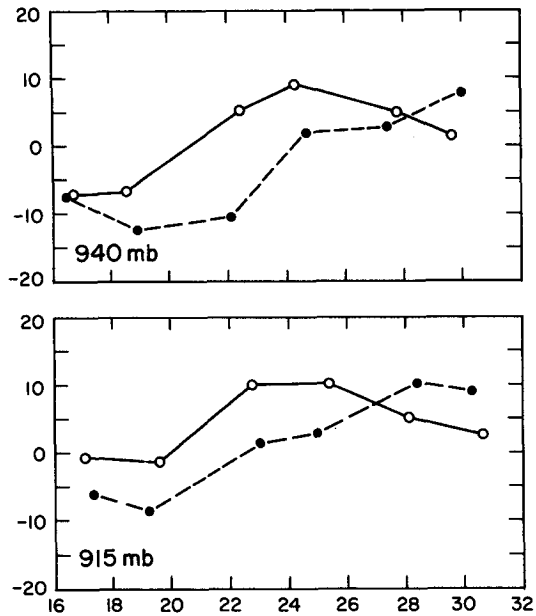


FIG. 12. Time evolution of $x$ (dashed line) and $y$ (solid line) ageostrophic wind components derived from airborne radar altimetry for 940 and 915 mb levels.

value of the geostrophic wind. The ability of the airborne measurement system to follow an isobaric surface is well documented (Rodi and Parish, 1988). Probably the single most important source of error in the geostrophic wind calculations is the uncertainty in local isobaric height changes.

The measurements presented seem to verify previous conceptions regarding the forcing and evolution of the LLJ. Diabatic heating and cooling of the sloping terrain produces distinct variations in the horizontal pressure gradient which match theoretical expectations. Although this isallobaric component is not insignificant, the largest forcing arises from the frictional decoupling mechanism. There appears to be a strong association between the rapid stabilization of the lower boundary layer and the onset of the LLJ. The case study observations and analysis suggest the frictional decrease and attendant inertial component dominate the behavior of this summertime LLJ.

## REFERENCES

Blackadar, A. K., 1957: Boundary-layer wind maxima and their significance for the growth of nocturnal inversions. *Bull. Amer. Meteor. Soc.*, **38,** 283–290.

Bonner, W. D., 1968: Climatology of the low level jet. *Mon. Wea. Rev.*, **96,** 833–850.

——, and J. Paegle, 1970: Diurnal variations in the boundary layer winds over the south central United States in summer. *Mon. Wea. Rev.*, **98,** 735–744.

Brown, E. N., M. A. Shapiro, P. J. Kennedy and C. A. Friehe, 1981: The application of airborne radar altimetry to the measurement of height and slope of isobaric surfaces. *J. Appl. Meteor.*, **20,** 1070–1074.

Clark, R. D., 1987: An observational and numerical study of the summertime, Great Plains low level jet. Ph.D. dissertation, University of Wyoming, 190 pp.

Haltiner, G. J., and F. L. Martin, 1957: *Dynamical and Physical Meteorology.* McGraw-Hill, 470 pp.

Hoecker, W. J., 1963: Three southerly low-level jet systems delineated by the Weather Bureau special pibal network of 1961. *Mon. Wea. Rev.*, **91,** 573–582.

——, 1965: Comparative physical behavior of southerly boundary layer jets. *Mon. Wea. Rev.*, **93,** 133–144.

Holton, J. R., 1967: The diurnal boundary layer wind oscillation above sloping terrain. *Tellus,* **19,** 199–205.

Izumi, Y., and M. L. Barad, 1963: Wind and temperature variations during development of a low level jet. *J. Appl. Meteor.*, **2,** 668–673.

Lettau, H. H., and B. Davidson, 1957: *Exploring the Atmosphere's First Mile. Vol. 2,* Pergamon Press, 578 pp.

——, and W. Schwerdtfeger, 1967: Dynamics of the surface-wind regime over the interior of Antarctica. *Antarct. J. U.S.*, **2,** 155–158.

McNider, R. T., and R. A. Pielke, 1981: Diurnal boundary-layer development over sloping terrain. *J. Atmos. Sci.*, **38,** 2198–2212.

Rodi, A. R., and T. R. Parish, 1988: Aircraft measurement of mesoscale pressure gradients and ageostrophic winds. *J. Atmos. Oceanic Technol.*, in press.

Shapiro, M. A., and P. J. Kennedy, 1981: Research aircraft measurements of jet stream geostrophic and ageostrophic winds. *J. Atmos. Sci.*, **38,** 2642–2652.

——, and ——, 1982: Airborne radar altimeter measurements of geostrophic and ageostrophic winds over irregular terrain. *J. Appl. Meteor.*, **21,** 1739–1746.

Uccellini, L. W., 1980: On the role of upper tropospheric jet streaks and leeside cyclogenesis in the development of low-level jets in the Great Plains. *Mon. Wea. Rev.*, **108,** 1689–1696.

——, and D. R. Johnson, 1979: The coupling of upper and lower tropospheric jet streams and implications for the development of severe convective storms. *Mon. Wea. Rev.*, **107,** 682–703.

Wexler, H., 1961: A boundary layer interpretation of the low level jet. *Tellus,* **13,** 368–378.